Mechano-Graded Electrodes Mitigate the Mismatch between Mechanical Reliability and Energy Density for Foldable Lithium-Ion Batteries

*Xiang Ge, Shengkai Cao, Zhisheng Lv, Zhiqiang Zhu, Yuxin Tang, Huarong Xia, Hongwei Zhang, Jiaqi Wei, Wei Zhang, Yanyan Zhang, Yi Zeng, Xiaodong Chen**

Dr. X. Ge
Department of Materials and Metallurgy, Guizhou University, Guiyang 550025, China

Dr. X. Ge, Dr. Z. Zhu, Dr. H. Xia, Dr. J. Wei, Dr. W. Zhang, Dr. Y. Zeng, Prof. X. Chen
Innovative Centre for Flexible Devices (iFLEX), Max Planck–NTU Joint Lab for Artificial Senses, School of Materials Science and Engineering, Nanyang Technological University, 50 Nanyang Avenue, 639798, Singapore
E-mail: chenxd@ntu.edu.sg

Dr. S. Cao, Dr. Z. Lv, Prof. X. Chen
Institute of Materials Research and Engineering, the Agency for Science, Technology and Research (A*STAR), 2 Fusionopolis Way, Innovis, #08-03, 138634, Singapore

Prof. X. Chen
Institute for Digital Molecular Analytics and Science (IDMxS), Nanyang Technological University, 59 Nanyang Drive, 636921, Singapore

Dr. Y. Tang, Dr. Y. Zhang, Dr. H. Zhang
College of Chemical Engineering, Fuzhou University, Fuzhou 350116, China

Keywords: Mechano-graded electrodes, flexibility, energy density, lithium‑ion batteries

Abstract

Flexible lithium-ion batteries (LIBs) with high energy density are highly desirable for wearable electronics. However, current approaches for designing flexible LIBs are diffcult to achieve the excellent flexibility and high energy density simultaneously. To mitigate the mismatch, mechano-graded electrodes with gradient-distributed maximum allowable strain are proposed to endow high-loading-mass slurry-coating electrodes with brilliant intrinsic flexibility without sacrificing energy density. As a proof-of-concept, the up-graded $LiNi_{1/3}Mn_{1/3}Co_{1/3}O_2$ cathodes (~15 mg cm^{-2}, ~70 μm) and graphite anodes (~8 mg cm^{-2}, ~105 μm) can tolerate an extremely low bending radius of 400 μm and 600 μm, respectively. Finite element analysis (FEA) reveals that, compared with conventionally homogeneous electrodes,

the flexibility of up-graded electrodes is enhanced by specifically strengthening the upper layer and avoiding crack initiation. Benefiting from this, the foldable pouch cell (required bending radius of ~600 μm) successfully realized a remarkable figure of merit (FOM, energy density versus bending radius) of 121.3 mWh cm^{-3}. Moreover, the up-graded electrodes-based pouch cells can deliver a stable power supply, even under various deformation modes, such as twisting, folding, and knotting. This work proposes new insights for harmonizing mechanics and electrochemistry of energy storage devices to achieve high energy density under flexible extremes.

1. Introduction

The ever-augmenting demands of flexible devices, such as skin electronics,[1] wearable devices,[2] and the internet of things[3] require energy storage systems with coordinated flexibility.[4] High energy density and mechanical reliability are two principles for pursuing the "Holy Grail" flexible power sources.[5] However, these two key indicators are difficult to be realized in a flexible energy storge device simultaneously. Li-ion batteries (LIBs) are one of the most promising candidate for powering flexible electronics due to their high energy density.[6] Extensive efforts have been devoted to fabricating flexible LIBs,[7] including macroscopic structural designs and flexible matrix development.[8] Typically, the rigid energy storage units or active materials are integrated with extrinsic flexible components,[8a, 9] such as constituting rigid-island soft-bridge,[8c] wavy,[8d] spine-like,[9b] fiber-like[4f, 5e] and lantern-like structures,[9c] or adapting porous polydimethylsiloxane (PDMS) sponge,[10] carbon fabrics,[3] silver nanowire,[11] carbon nanotubes (CNTs),[11-12] carbon nanofibers (CNFs)[13] and graphene as flexible substrates.[14] Although these structures enable a stable power supply under deformation,[15] extrinsic inactive components or limited loading mass of active materials have to be employed to provide sufficient mechanical reliability, thus trading off the energy density.[16] Besides, most mechanically flexible materials would degrade gradually either at

the anode or at the cathode side due to the highly reductive or oxidative environment in a full LIB with a voltage higher than 3.5 V under long-term service. Moreover, foldability with an extremely low bending radius (500-1000 μm) scale remains difficult to be achieved in reported flexible LIBs.[8b, 17] Therefore, it is highly desirable to develop alternative strategies for manufacturing electrodes with superior intrinsic flexibility while maintaining high energy density.[18]

Distinguished from flexible electrodes with redundant mechanical structures, commercialized slurry-coating electrodes primarily consist of electrochemically active coating film.[19, 20] The intrinsic flexibility of the electrodes depends on the maximum allowable strain, which is related to the binder ratio (**Figure 1**a; Figure S1, Supporting Information).[22] The maximum allowable strain of the electrodes can be enhanced by increasing the binder ratio, whereas followed by inferior energy density due to the reduced ratio of active materials. Unfortunately, the commercialized electrodes usually require a high active materials ratio (> 90%) and a high loading mass (1.5~4 mAh cm^{-2}, 70-150 μm, depending on the application scenario) to deliver a high energy density.[19, 20] Such electrodes thus normally suffer from poor mechanical flexibility due to mechanical fracture or peeling-off under bending, folding or other deformation conditions, compared with thin electrodes with low loading mass.[21] Hence, realizing flexible high-energy-density LIBs based on the slurry-coating electrodes is still challenging due to the contradictory requirements of high energy density (high loading mass and low binder ratio) and superb intrinsic flexibility (low loading mass and high binder ratio).[23]

To rationally mitigate the mismatch between mechanical reliability and high energy density of the electrodes, the bending strain distribution is depicted by

$$\varepsilon = d/\rho \quad (1)$$

where ε is the bending strain, ρ and d is the bending radius and the thickness of the electrode, respectively.[24, 25] Figure 1b shows the strain distribution at different bending radii. Upon

bending, the strain increases with the distance from the substrate and reaches the maximum at the top surface. When a low bending radius is exerted on homogeneous electrodes, the constant maximum allowable strain would be exceeded by bending strain at the intersection point (Figure 1c). The electrode layer on the right of the intersection point cannot tolerate the bending strain, thus inducing the mechanical fracture. Accordingly, the flexibility of electrodes can be improved if the distribution of the maximum allowable strain is aligned with the gradient distribution of the strain induced by bending (Figure 1d).

Inspired by this, mechano-graded electrodes, in which the distribution of maximum allowable strain is regulated to align with the gradient-distributed strain induced by bending (up-graded electrodes), thus increasing the flexibility of the electrodes without sacrificing energy density, are proposed. As control groups, the homogeneous and down-graded electrodes with constant and lower maximum allowable strain at the upper surface layer, respectively, are studied for comparison. Such a mechano-up-graded structure would enable the electrode to tolerate higher strain upon bending while not sacrificing the energy density. As a proof-of-concept, the up-graded 70 μm cathodes (~15 mg cm^{-2}, $LiNi_{1/3}Mn_{1/3}Co_{1/3}O_2$, NMC) and 105 μm anodes (~8 mg cm^{-2}, graphite) can tolerate an extremely low bending radius of 400 μm and 600 μm, respectively. The 60 mAh rectangular pouch cells based on the up-graded electrodes with areal specific capacity of ~2 mAh cm^{-2} can achieve an impressive figure of merit (FOM, energy density versus bending radius) value of 121.3 mWh cm^{-3}, indicating the successful optimization of flexibility without sacrificing the energy density. The pouch cell can retain ~96.0% of initial capacity after 50 cycles under repeated folding-releasing conditions, higher than that of pouch cells using homogeneous (90.9%) and down-graded electrodes (89.5%). Noteworthy, when the pouch cells are subjected to cycling after the above folding-releasing process for another 500 cycles, the accumulated damages lead to more severe capacity decay for pouch cells using homogeneous (79.7% retention) or down-graded electrodes (57.2% retention) than up-graded electrodes (92.3% retention). Besides, the

protocol is compatible with industrial equipment and can be easily scaled up because the process can be achieved with a normal slurry coating method and involves only commercially available chemicals. The strategy of mechano-graded electrodes is not limited to specific material systems, thus being generally applicable for fabricating other flexible power supply components with improved bendability while maintaining high energy density.

2. Results and Discussion

The mechano-graded electrodes are rationally conceived by controlling the distribution of the binder ratio via a repeated coating-drying process (**Figure 2**a-c, detailed methods given in the Supporting Information). Both mechano-graded and homogeneous electrodes have an industrial low average binder ratio of less than 5% and areal capacity of ~2 mAh cm^{-2}. The gradient distribution of the binder ratio can be verified by EDX mapping performed on the cross section (Figure S2, Supporting Information). The increased intensity for the characteristic F $K_{\alpha}1$ signal of the polyvinylidene fluoride (PVDF) binder from the bottom to the top layer indicates the successful fabrication of up-graded electrodes. Figure 2d and 2e show the representative optical images of bent cathodes (bending radius of 400 μm) and anodes (bending radius of 600 μm). Under this condition, the up-graded electrodes can tolerate such extreme bending while obvious cracks are observed for homogeneous and down-graded electrodes. Additional parallel experiment was conducted to prevent the interference from manual error (Figure S3, Supporting Information). These results indicate that the up-graded electrodes with gradient-distributed maximum allowable strain can improve mechanical reliability while maintaining the high loading mass and active materials ratio.

The bendability of the mechano-graded and homogeneous electrodes can be quantified by using the maximum curvature (**Figure 3**a, b; Figure S4, Supporting Information). The maximum curvature is equal to the reciprocal of minimum bending radius. To prepare the bended electrodes with certain bending radius, we have stacked different layers of double-

sided tapes, and then bent electrodes convexly onto the tape stacks (Figure S5, Supporting Information). Because each layer of the double-sided tape has a thickness of about 200 μm, the bending radius is equal to 100 μm multiplied by the number of layers. By bending electrodes onto tapes with different layers and observing them under an optical microscope, we can quantify the minimum bending radius (number of tape layers) before the crack initiation. This technique enables the accurate quantification of electrode bendability at a step size of 100 μm. The contour plots in Figure 3a and 3b show the quantified bendability of homogeneous electrodes. The maximum allowable strain evaluated by this method is higher than that tested by peeling off the active materials layer and applying tensile stretch test (Figure S1) because it avoids the peeling off process which could introduce defect to the electrode especially when the binder ratio is low (< 5.0%). Notably, both the industrial up-graded cathodes and anodes exhibit higher maximum bending curvatures than down-graded electrodes (cathode: 0.0033 μm^{-1} vs. 0.0017 μm^{-1}, anode: 0.0020 μm^{-1} vs. 0.0010 μm^{-1}) and homogeneous electrodes, indicating their superior bendability. In addition, cathodes are generally more mechanically robust (higher maximum curvature) than anodes under the same conditions, because the PVDF binder is less adhesive to graphite compared to NMC.[29] The spherical morphology of NMC secondary particle should also be more mechanically favorable compared to the irregular shape of graphite (Figure S6 and S7, Supporting Information). This is also identified by FEA simulation (Figure S8, Supporting Information). Moreover, the up-graded electrodes with a strengthened top layer can provide better anti-scratching properties, which is useful during electrode handling (Figure S9, Supporting Information).

To correlate the superior flexibility with gradient-distribution maximum allowable strain, the mechanical failure mechanism of electrodes under bending was investigated by finite element analysis (FEA, Figure 3c). The structure of electrodes can be considered as a special bilayer beam, for which the theoretical quantification of the strain and stress distribution is already well established.[26] Considering that the tensile strain is more

destructive than compressive strain for the active material layer, here we focus on the convex bending process where it would introduce tensile strain above the neutral plane and compressive strain below the neutral plane.[27] In the case of a pure bending process without shear strain, the bending curvature remains constant. The cross-section plane remains to be planar without torsion or warping. The tensile or compressive strain at a given location would be linearly related to its distance to the neutral plane (Equation (2)):

$$\varepsilon(y) = \kappa H(y) = \kappa\left(h - y\right) \quad (2)$$

$\varepsilon(y)$ is the strain related to the y-coordinate. κ is the bending curvature inversely proportional to the bending radius ρ, $\kappa = 1/\rho$. $H(y)$ is the vertical distance between the studied location and the neutral plane. h is the y-coordinate of the neutral plane. Once the position of the neutral plane is determined, the strain distribution at each curvature can be calculated. The position of the neutral plane depends on the thickness and Young's modulus of the film and the substrate. For common electrodes, the Young's modulus of the metallic substrate is in the order of 10^2 GPa. The maximum allowable strain of the active material layer is highly dependent on the binder ratio. When the binder ratio is less than 10%, the Young's modulus of the active materials layer is in the order of 10^0 MPa. Because the Young's modulus values between the active materials layer and the substrate are highly different (10^3 to 10^5 times), the mechanical neutral plane of electrodes should be near the original neutral plane of the metallic substrate. This conclusion applies to various conditions, including the homogeneous or multi-layer film when being subjected to pure bending in both the elastic and the plastic ranges. The details for quantifying the position of the neutral plane and the strain distribution is discussed in Scheme S1-S4, Supporting Information. Accordingly, FEA was performed to simulate the bending fracture process of electrodes (Figure 3c; Movie S1, Supporting Information). The thickness of the active material layer film is set to be 150 μm to better visualize the strain at the cross section, while the practical data are used for other parameters (details given in the Supporting Information). Based on the simulation results, the bending

fracture process can be described with three stages. At the initial stage, the external bending leads to the gradual increase of the bending curvature. The much harder substrate would drag the neutral plane downward below the substrate-film interface.[28] Therefore, the whole active material layer would have tensile bending strain that maximizes at the top layer. Once a crack forms at the top layer, the strain would redistribute and localize at the crack tip, thus leading to the fast propagation of the crack downward. Finally, the crack would reach the interface between the metallic substrate and the active material layer. At this stage, the strain would distribute at the interface, leading to the peeling-off of the active material layer.

To verify the above-described bending fracture process is the dominating mechanism that limits the bendability of electrodes, we used an optical microscope to observe the cross section of the bent electrodes with a controlled bending radius. Typical optical images of electrodes with various thicknesses are being bent at various curvatures (Figure S10a-c, Supporting Information). All the cracks have a wedge-like shape, consistent with the simulation results shown in Figure 3a. Under more severe bending (Figure S10e, Supporting Information), the active material layer recovers to a near-straight shape, which are identical to the FEA results (Figure S10d, Supporting Information). These observations confirm that the crack initiation at the top surface and further strain redistribution process is the dominating mechanism for electrode failure under bending. For pouch cells with a pair of electrodes, the active material layer and the metallic substrate are bonded, while other interfaces can be frictionally slidable for the shear strain to release. The bending process leads to convex bending of one electrode and concave bending of its counter electrode with a similar bending curvature (Figure S5f). Alleviating the destructive effect during the convex bending is the key to enhancing the bendability of pouch cells. Based on above analysis, the up-graded electrodes with gradient-increased maximum allowable strain from the bottom (contact current collector) to the top layer can suppress the crack initiation and propagation, and thus can simultaneously achieve exceptional flexibility and high loading mass.

Besides the superior mechanical flexibility, excellent electrochemical performance is another key indicator for flexible LIBs. Cyclic Voltammetry (CV) curves (Figure S11a, Supporting Information) and charge/discharge curves (Figure S11b, c Supporting Information) show that the up-graded graphite/Li half-cell, up-graded NMC/Li half-cell and the up-graded NMC/up-graded graphite full cell function properly as expected (a redox pair and charge/discharge plateau in the range of 3.6-4.3 V).[30] Electrochemical impedance spectrum (EIS, Figure S12, Supporting Information) shows that both up-graded cathodes and anodes have analogous features, but slightly lower impedance compared with homogeneous or down-graded electrodes. This indicates that the up-graded electrodes maintained their electrochemical kinetics while the flexibility is obviously improved. To compare the cycling stability of electrodes after folding, defective cathodes and anodes were prepared by convexly bending with three horizontal lines and three vertical lines, respectively (Figure S13, Supporting Information). The bending curvature is controlled with a spacer. For homogeneous electrodes and down-graded electrodes, the folding damage or peeling-off can be directly visualized while up-graded electrodes can maintain their structural integrity. The pristine electrodes and folded electrodes are then assembled in coin cells. Figure S14 (Supporting Information) shows the comparison of the cycling stability of cathodes and anodes before and after folding, respectively. The discharge capacity at the first cycle and the capacity retention after 220 cycles of different pristine electrodes and folded (bending radius of 370 μm for cathodes and 485 μm for anodes) electrodes are summarized in **Figure 4**a. For unfolded cathodes and anodes, up-graded, homogeneous and down-graded electrodes have similar discharge capacity (143.6, 144.1 and 145.5 mAh g^{-1} for the cathodes, respectively; 343.6, 331.3 and 350.5 mAh g^{-1} for the anodes, respectively) and cycling stability (82.7%, 80.5% and 79.9% for the cathodes, respectively; 88.0%, 88.7% and 87.2% for the anodes, respectively) regardless of coating methods. For folded electrodes, the up-graded cathode and anode both show higher initial discharge capacity (131 mAh g^{-1} for cathode and 337 mAh g^{-1}

for anode) than the homogeneous (124 mAh g^{-1} for the cathode and 303 mAh g^{-1} for the anode) and down-graded (119 mAh g^{-1} for the cathode and 291 mAh g^{-1} for the anode) electrodes because of less electrode damage during folding. Noteworthy, the up-graded electrodes also show better cycling stability (85% for the cathode and 89% for the anode) than the homogeneous electrodes (76% for the cathode and 79% for the anode) and down-graded electrodes (73% for the cathode and 65% for the anode) at 220th cycle. The normalized capacity retention percentage of folded electrodes is higher than that of unfolded electrode because the folding process also leads to lower initial discharge capacity despite the absolute discharge capacity of folded cathode at the 220th cycle is lower. The higher long-cycle capacity retention of up-graded electrodes is because of fewer defects that could deteriorate the electrode integrity during repeated volume change during lithium insertion/extraction.

A figure of merit (FOM) of areal energy density versus minimum bending radius ($FOM = E_a/r$) is employed to standardize the comparison of various state-of-the-art designs (Figure 4b) of flexible LIBs.[25, 31] The FOM value can provide an indicator to evaluate the intrinsic performance of flexible energy storage system regardless of their geometrical parameters. For rational comparison, the FOM only includes batteries with 2D isotropic bending behavior (macroscopically deformable batteries like spine-like batteries are not included because of the anisotropic bending radius). Conventional coin cells and cylinder cells are not bendable due to the rigid stainless-steel package. Various flexible battery systems, including metal mesh LIBs, paper LIBs, and fabric LIBs,[32] can achieve a bending radius in the range of 0.1 to 10 cm and an areal energy density of 1 to 10 mWh cm^{-2}, providing FOM values ranging from 1 to 100. Noteworthy, the pouch cells using the up-graded NMC cathodes and graphite anodes can provide an areal energy density of about 7.28 mWh cm^{-2} with a minimum bending radius of 0.06 cm (limited by the anode side), indicating a remarkable FOM of 121.3 mWh cm^{-3} (Figure S15, Supporting Information; FOM values for homogeneous and down-graded electrodes are calculated to be 90.9 and 72.6 mWh/cm^3,

respectively). All these results verified that the up-graded electrodes can enhance the intrinsic flexibility of practical high-loading-mass electrodes.

Due to the high compatibility with commercialized raw materials and existing industrial technology, the manufacturing process of mechano-graded electrodes can be easily scaled up (Figure S16, Supporting Information). The up-graded electrodes-based flexible pouch cells with an areal capacity of ~2 mAh cm^{-2} were thus successfully assembled (**Figure 5**). The rectangular pouch cells were fabricated using 1.2 cm × 25 cm electrodes with a total capacity of ~60 mAh. The flexible pouch cells were first stabilized for 20 charge/discharge cycles before evaluating the electrochemical stability. In the following 20-50 cycles, the cells were cycled under repeated folding and releasing conditions (Figure 5a). For pouch cells using homogeneous electrodes or down-graded electrodes, there is an obvious abrupt change in the available capacity during the first releasing process, while the capacity of pouch cells using up-graded electrodes does not show obvious change. The initial three folding-releasing cycles have a huge effect on the battery lifespan. In the following 50-520 cycles, the up-graded electrodes exhibit superior long-term stability (92.3% retention at the 520^{th} cycle, Figure 5b). By contrast, the capacity of pouch cells using homogeneous electrodes and down-graded electrodes continuously decay (79.7% and 57.2% retention at the 520^{th} cycle, respectively). This is because the initial folding-releasing processes not only leads to the capacity loss in the homogeneous and down-graded electrodes, but also the formation and expansion of regional defects where the overcharge would occur during the subsequent electrochemical charge/discharge.[33] It is worth mentioning that more folding-releasing cycles won't result in immediate and obvious decay unless the folding positions are increased (Figure S17, Supporting Information). To further demonstrate the reliability of the up-graded electrode-based pouch cells to function under various conditions, they are connected to a chain of white LED and then subjected to twisting, folding and knotting (Figure 5c and Movie

S2, Supporting Information). The LEDs keep illuminating stably, indicating the stable output from the pouch cells.

3. Conclusion

In summary, mechano-graded electrodes with a gradient-distributed maximum allowable strain have been rationally conceived and fabricated to mitigate the mismatch between the mechanical flexibility and energy density. Based on FEA analysis, the up-graded electrodes with a strengthened upper layer can tolerate the gradient-distributed strain induced by bending, thus avoiding crack initiation and subsequent electrodes failure. Benefiting from this, the up-graded cathodes and anodes can endure an extremely low bending radius of 400 μm and 600 μm, respectively. Furthermore, the 60 mAh up-graded electrode-based pouch cells with an areal capacity of ~2 mAh cm^{-2} exhibit a higher capacity retention of ~ 92.3% at the 550^{th} cycle under repeated folding-releasing, much better than that of homogeneous electrodes (79.7%) and down-graded electrodes (57.2%). Noteworthy, the up-graded electrode-based LIBs enable an FOM value of 121.3 mWh cm^{-3}, proving the superior intrinsic flexibility of high-energy-density electrodes. The pouch cells can still provide a stable power supply under various deformation modes, such as folding, twisting and knotting. Moreover, the manufacturing process of mechano-graded electrodes is highly compatible with industrial battery production. Such mechano-graded design should not only enable the commercialization of flexible LIBs, but also be useful for designing other flexible electronic devices with superior flexibility while not sacrificing other significant performance.

4. Experimental Section/Methods

The detailed experimental process is available in the Supporting Information.

Supporting Information

Supporting Information is available from the Wiley Online Library or from the author.

Acknowledgements

X.G. and S.C. contributed equally to this work. This work was supported by the Agency for Science, Technology and Research (A*STAR) under its AME Programmatic Funding Scheme (Project #A18A1b0045). Xiang Ge acknowledges the support from National Science Foundation of China (52262030) and Natural Science Foundation of Guizhou Science and Technology Department (QKHJC-ZK[2021]-YB257).

Received: ((will be filled in by the editorial staff))
Revised: ((will be filled in by the editorial staff))
Published online: ((will be filled in by the editorial staff))

References

[1] Y. R. Jeong, G. Lee, H. Park, J. S. Ha, *Acc. Chem. Res.* **2018**, *52*, 91.

[2] a) G. Zhou, F. Li, H.-M. Cheng, *Energy Environ. Sci.* **2014**, *7*, 1307; b) Q. Li, G. Chen, Y. Cui, S. Ji, Z. Liu, C. Wan, Y. Liu, Y. Lu, C. Wang, N. Zhang, Y. Cheng, K.-Q. Zhang, X. Chen, *ACS Nano* **2021**, *15*, 9955; c) J. Wang, C. Wang, P. Cai, Y. Luo, Z. Cui, X. J. Loh, X. Chen, *ACS Nano* **2021**, *15*, 18671.

[3] J. Chang, J. Shang, Y. Sun, L. K. Ono, D. Wang, Z. Ma, Q. Huang, D. Chen, G. Liu, Y. Cui, *Nat. Commun.* **2018**, *9*, 4480.

[4] a) W.-J. Song, S. Lee, G. Song, H. B. Son, D.-Y. Han, I. Jeong, Y. Bang, S. Park, *Energy Storage Mater.* **2020**, *30*, 260; b) J. He, C. Lu, H. Jiang, F. Han, X. Shi, J. Wu, L. Wang, T. Chen, J. Wang, Y. Zhang, *Nature* **2021**, *597*, 57; c) J. Wei, L. Zhong, H. Xia, Z. Lv, C. Diao, W. Zhang, X. Li, Y. Du, S. Xi, M. Salanne, X. Chen, S. Li, *Adv. Mater.* **2022**, *34*,

2107439; d) Q. Fu, S. Hao, L. Meng, F. Xu, J. Yang, *ACS Nano* **2021**, *15*, 18469; e) S. Kang, S. Y. Hong, N. Kim, J. Oh, M. Park, K. Y. Chung, S.-S. Lee, J. Lee, J. G. Son, *ACS Nano* **2020**, *14*, 3660; f) J. He, C. Lu, H. Jiang, F. Han, X. Shi, J. Wu, L. Wang, T. Chen, J. Wang, Y. Zhang, H. Yang, G. Zhang, X. Sun, B. Wang, P. Chen, Y. Wang, Y. Xia, H. Peng, *Nature* **2021**, *597*, 57.

[5] a) D. G. Mackanic, M. Kao, Z. Bao, *Adv. Energy Mater.* **2020**, *10*, 2001424; b) D. Wang, C. Han, F. Mo, Q. Yang, Y. Zhao, Q. Li, G. Liang, B. Dong, C. Zhi, *Energy Storage Mater.* **2020**, *28*, 264; c) T. Yang, J. Xia, Z. Piao, L. Yang, S. Zhang, Y. Xing, G. Zhou, *ACS Nano* **2021**, *15*, 13901; d) J. Zhang, X. Fan, X. Meng, J. Zhou, M. Wang, S. Chen, Y. Cao, Y. Chen, C. W. Bielawski, J. Geng, *ACS Nano* **2021**, *15*, 8870; e) M. Liao, C. Wang, Y. Hong, Y. Zhang, X. Cheng, H. Sun, X. Huang, L. Ye, J. Wu, X. Shi, X. Kang, X. Zhou, J. Wang, P. Li, X. Sun, P. Chen, B. Wang, Y. Wang, Y. Xia, Y. Cheng, H. Peng, *Nature Nanotechnology* **2022**, *17*, 372.

[6] a) Y. Liu, R. Zhang, J. Wang, Y. Wang, *iScience* **2021**, *24*, 102332; b) X. Yan, T. Li, Y. Xiong, X. Ge, *Energy Storage Mater.* **2021**, *36*, 213; c) W. Zhang, Y. Sun, H. Deng, J. Ma, Y. Zeng, Z. Zhu, Z. Lv, H. Xia, X. Ge, S. Cao, Y. Xiao, S. Xi, Y. Du, A. Cao, X. Chen, *Adv. Mater.* **2020**, *32*, 2000496; d) L. Zhang, X. Qin, S. Zhao, A. Wang, J. Luo, Z. L. Wang, F. Kang, Z. Lin, B. Li, *Adv. Mater.* **2020**, *32*, 1908445; e) H. Xia, W. Zhang, S. Cao, X. Chen, *ACS Nano* **2022**, *16*, 8525; f) L. Xue, S. V. Savilov, V. V. Lunin, H. Xia, *Adv. Funct. Mater.* **2018**, *28*, 1705836; g) Q. Chen, S. Sun, T. Zhai, M. Yang, X. Zhao, H. Xia, *Adv. Energy Mater.* **2018**, *8*, 1800054.

[7] a) H. Yang, Z. Feng, X. Teng, L. Guan, H. Hu, M. Wu, *InfoMat* **2021**, *3*, 631; b) S. Y. Hong, S. M. Jee, Y. Ko, J. Cho, K. H. Lee, B. Yeom, H. Kim, J. G. Son, *ACS Nano* **2022**, *16*, 2271.

[8] a) L. Mao, Q. Meng, A. Ahmad, Z. Wei, *Adv. Energy Mater.* **2017**, *7*, 1700535; b) G. Qian, X. Liao, Y. Zhu, F. Pan, X. Chen, Y. Yang, *ACS Energy Lett.* **2019**, *4*, 690; c) S. Xu, Y.

Zhang, J. Cho, J. Lee, X. Huang, L. Jia, J. A. Fan, Y. Su, J. Su, H. Zhang, *Nat. Commun.* **2013**, *4*, 1543; d) W. Liu, J. Chen, Z. Chen, K. Liu, G. Zhou, Y. Sun, M. S. Song, Z. Bao, Y. Cui, *Adv. Energy Mater.* **2017**, *7*, 1701076.

[9] a) X. Liao, C. Shi, T. Wang, B. Qie, Y. Chen, P. Yang, Q. Cheng, H. Zhai, M. Chen, X. Wang, *Adv. Energy Mater.* **2018**, 1802998; b) G. Qian, B. Zhu, X. Liao, H. Zhai, A. Srinivasan, N. J. Fritz, Q. Cheng, M. Ning, B. Qie, Y. Li, S. Yuan, J. Zhu, X. Chen, Y. Yang, *Adv. Mater.* **2018**, *30*, 1704947; c) Z. Lv, Y. Tang, Z. Zhu, J. Wei, W. Li, H. Xia, Y. Jiang, Z. Liu, Y. Luo, X. Ge, Y. Zhang, R. Wang, W. Zhang, X. J. Loh, X. Chen, *Adv. Mater.* **2018**, *30*, 1805468.

[10] W. Liu, Z. Chen, G. Zhou, Y. Sun, H. R. Lee, C. Liu, H. Yao, Z. Bao, Y. Cui, *Adv. Mater.* **2016**, *28*, 3578.

[11] a) C. Hwang, W. J. Song, J. G. Han, S. Bae, G. Song, N. S. Choi, S. Park, H. K. Song, *Adv. Mater.* **2018**, *30*, 1705445; b) L. Hu, J. W. Choi, Y. Yang, S. Jeong, F. La Mantia, L.-F. Cui, Y. Cui, *Proc. Natl. Acad. Sci. U.S.A.* **2009**, *106*, 21490.

[12] H. Lee, J. K. Yoo, J. H. Park, J. H. Kim, K. Kang, Y. S. Jung, *Adv. Energy Mater.* **2012**, *2*, 976.

[13] Y. Ding, X. Guo, Y. Qian, L. Zhang, L. Xue, J. B. Goodenough, G. Yu, *Adv. Mater.* **2019**, *31*, 1806956.

[14] a) K. Chen, J. Cao, Q. Lu, Q. Wang, M. Yao, M. Han, Z. Niu, J. Chen, *Nano Res.* **2018**, *11*, 1345; b) T. Hoshide, Y. Zheng, J. Hou, Z. Wang, Q. Li, Z. Zhao, R. Ma, T. Sasaki, F. Geng, *Nano Lett.* **2017**, *17*, 3543.

[15] Y.-H. Zhu, X. Yang, D. Bao, X.-F. Bie, T. Sun, S. Wang, Y.-S. Jiang, X.-B. Zhang, J.-M. Yan, Q. Jiang, *Joule* **2018**, *2*, 736.

[16] a) J. M. Son, S. Oh, S. H. Bae, S. Nam, I. K. Oh, *Adv. Energy Mater.* **2019**, *9*, 1900477; b) L. Li, Z. P. Wu, H. Sun, D. Chen, J. Gao, S. Suresh, P. Chow, C. V. Singh, N. Koratkar, *ACS Nano* **2015**, *9*, 11342.

[17] X. Liu, J. Guo, T. Liu, J. Zhang, Z. Jia, C. Zhang, *Energy Storage Mater.* **2021**, *35*, 520.

[18] a) Q. Yang, A. Chen, C. Li, G. Zou, H. Li, C. Zhi, *Matter* **2021**, *4*, 3146; b) X. Li, S. Ling, L. Zeng, H. He, X. Liu, C. Zhang, *Adv. Energy Mater.* **2022**, *12*, 2200233.

[19] A. Kraytsberg, Y. Ein‐Eli, *Adv. Energy Mater.* **2016**, *6*, 1600655.

[20] Y. Kuang, C. Chen, D. Kirsch, L. Hu, *Adv. Energy Mater.* **2019**, *9*, 1901457.

[21] Y. Zhang, F. Li, K. Yang, X. Liu, Y. Chen, Z. Lao, K. Mai, Z. Zhang, *Adv. Funct. Mater.* **2021**, *31*, 2100434.

[22] M. Zheng, Y. Wang, J. Reeve, H. Souzandeh, W.-H. Zhong, *Energy Storage Mater.* **2018**, *14*, 149.

[23] J. Chang, Q. Huang, Y. Gao, Z. Zheng, *Adv. Mater.* **2021**, 2004419.

[24] E. Sahraei, R. Hill, T. Wierzbicki, *J. Power Sources* **2012**, *201*, 307.

[25] J. Peng, G. J. Snyder, *Science* **2019**, *366*, 690.

[26] Z. Suo, E. Ma, H. Gleskova, S. Wagner, *Appl. Phys. Lett.* **1999**, *74*, 1177.

[27] S. I. Park, J. H. Ahn, X. Feng, S. Wang, Y. Huang, J. A. Rogers, *Adv. Funct. Mater.* **2008**, *18*, 2673.

[28] W. Jo, H. Lee, Y. Lee, B.-S. Bae, T.-S. Kim, *Adv. Eng. Mater.* **2021**, *23*, 2001280.

[29] M. Yoshio, R. J. Brodd, A. Kozawa, *Lithium-ion batteries*, Vol. 1, Springer, **2009**.

[30] a) N. Nitta, F. Wu, J. T. Lee, G. Yushin, *Mater. Today* **2015**, *18*, 252; b) J. P. Pender, G. Jha, D. H. Youn, J. M. Ziegler, I. Andoni, E. J. Choi, A. Heller, B. S. Dunn, P. S. Weiss, R. M. Penner, *ACS Nano* **2020**, *14*, 1243.

[31] J. Chang, Q. Huang, Z. Zheng, *Joule* **2020**, *4*, 1346.

[32] K. K. Fu, J. Cheng, T. Li, L. Hu, *ACS Energy Lett.* **2016**, *1*, 1065.

[33] a) D. Mohanty, E. Hockaday, J. Li, D. K. Hensley, C. Daniel, D. L. Wood, *J. Power Sources* **2016**, *312*, 70; b) L. David, R. E. Ruther, D. Mohanty, H. M. Meyer, Y. Sheng, S. Kalnaus, C. Daniel, D. L. Wood, *Appl. Energy* **2018**, *231*, 446.

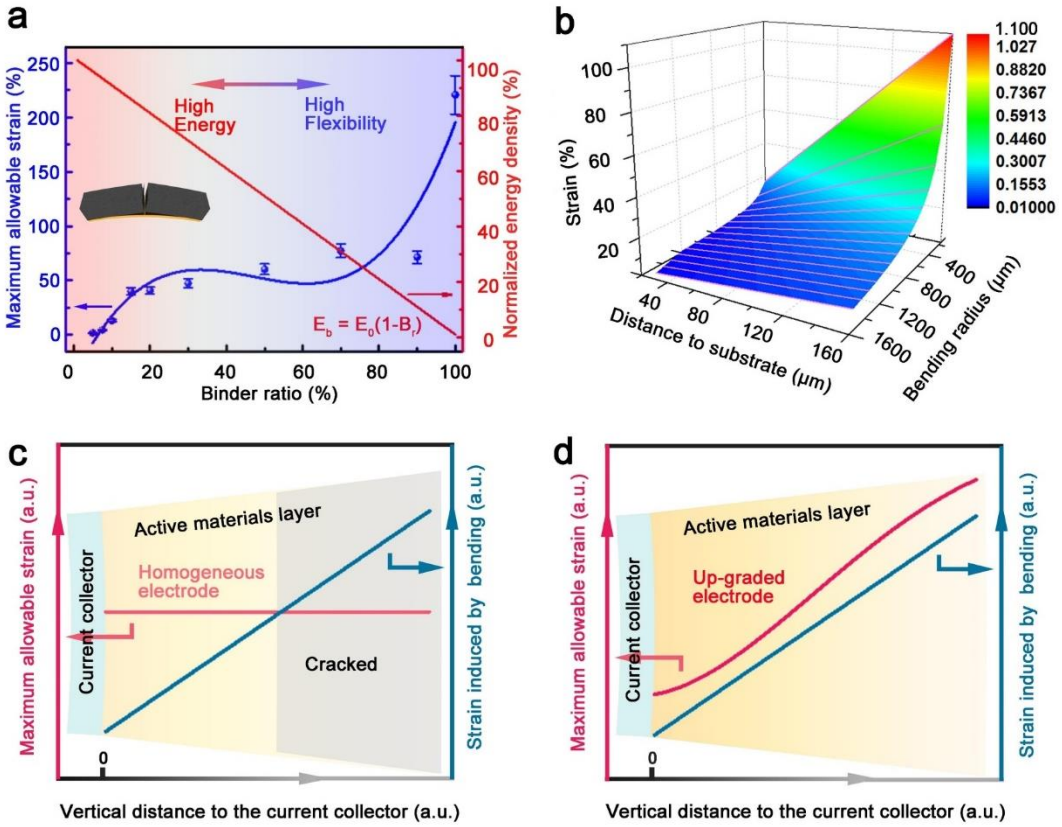

Figure 1. Design principles of mechano-graded electrodes with gradient-distributed maximum allowable strain. a) The mismatch between maximum allowable strain before rupture and energy density for homogeneous electrodes at various binder ratios. The energy density is calculated based on the active materials ratio. The energy density of the electrode (E_b) is calculated based on maximum energy density without binder (E_0) and the binder ratio (B_r) of the studied electrode. The maximum allowable strain is evaluated based on the tensile stretch results of electrodes with various binder ratios. b) Strain distribution analysis at various bending radii. The normal strain would always maximize at the top layer. c and d) The distribution of intrinsic maximum allowable strain of active materials layer and strain induced by convex bending for homogeneous (c) and up-graded (d) electrodes, respectively.

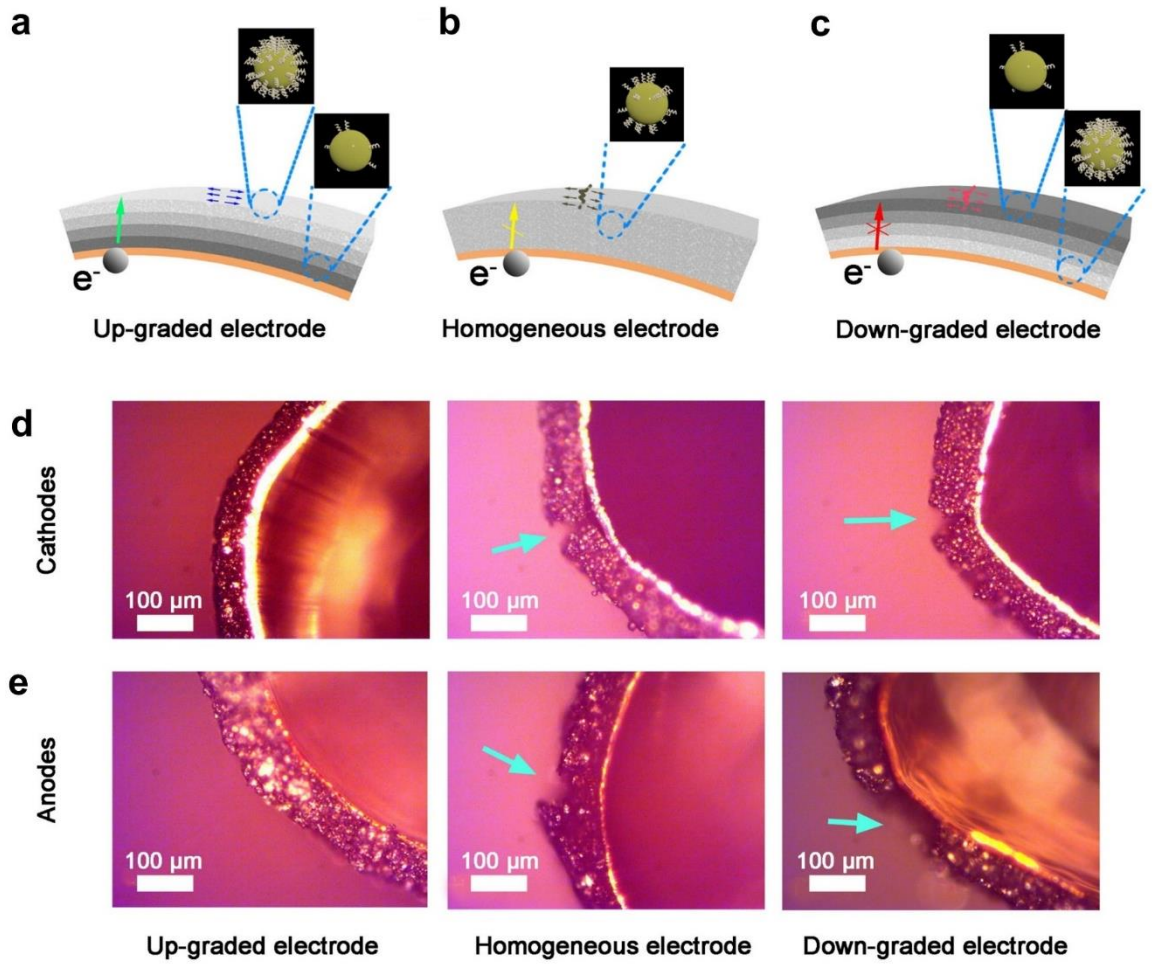

Figure 2. Schematic illustrations and intrinsic bendability of up-graded, homogeneous and down-graded electrodes. a-c) Schematic illustration of up-graded, homogeneous, and down-graded electrodes. The gradient distribution of binders enables simultaneous optimization of bendability and electronic conductivity in the up-graded electrode (a) than homogeneous (b) or down-graded electrode (c). d and e) Optical images showing the bendability of homogeneous or mechano-graded electrodes. The electrode thickness is 70 ± 5 μm for the cathodes (d) and 105 ± 10 μm for the anodes (e). The bending radius is kept at 400 μm for the cathodes and 600 μm for the anodes.

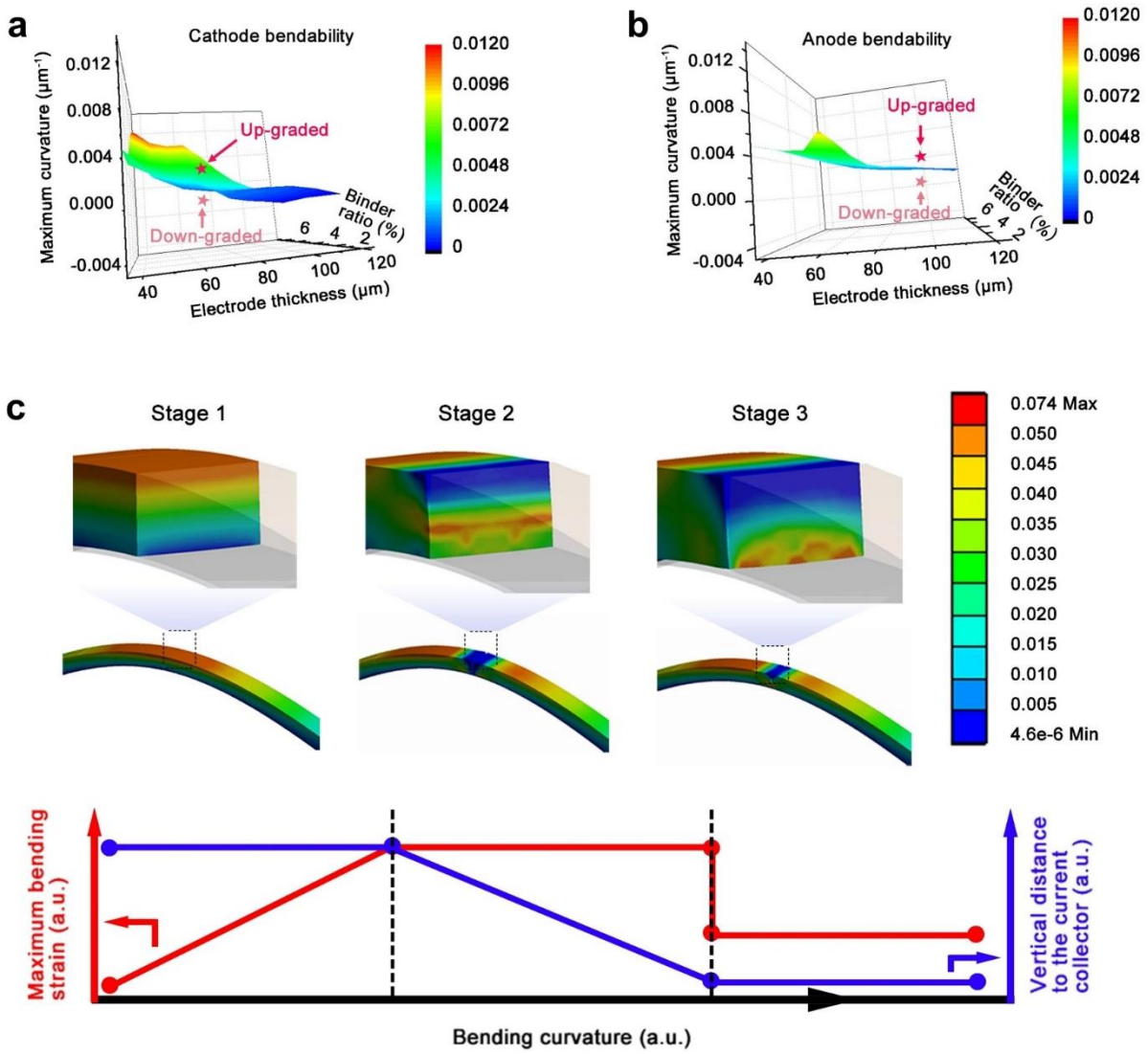

Figure 3. The quantified bendability and mechanical failure mechanism of electrodes. a and b) Comparison of the maximum curvature for mechano-graded and homogeneous cathodes (a) and anodes (b), respectively. The bendability of homogeneous electrodes with different binder ratio and electrode thickness are depicted by the 3D contour plots. The quantification of the maximum curvature for the electrode can be realized by gradually decreasing the bending radius and recording the bending radius when the crack initiates. The up-graded design shows improved bendability for both cathodes and anodes. c) FEA results of the strain distribution in the electrodes during bending. At the initial stage, the maximum strain concentrates on the top layer. Once the crack initiates, the strain would localize at the crack tip and lead to fast propagation of the crack. When the fracture reaches the substrate, the maximum strain would propagate along the interface between the active material layer and the substrate, leading to the peeling off.

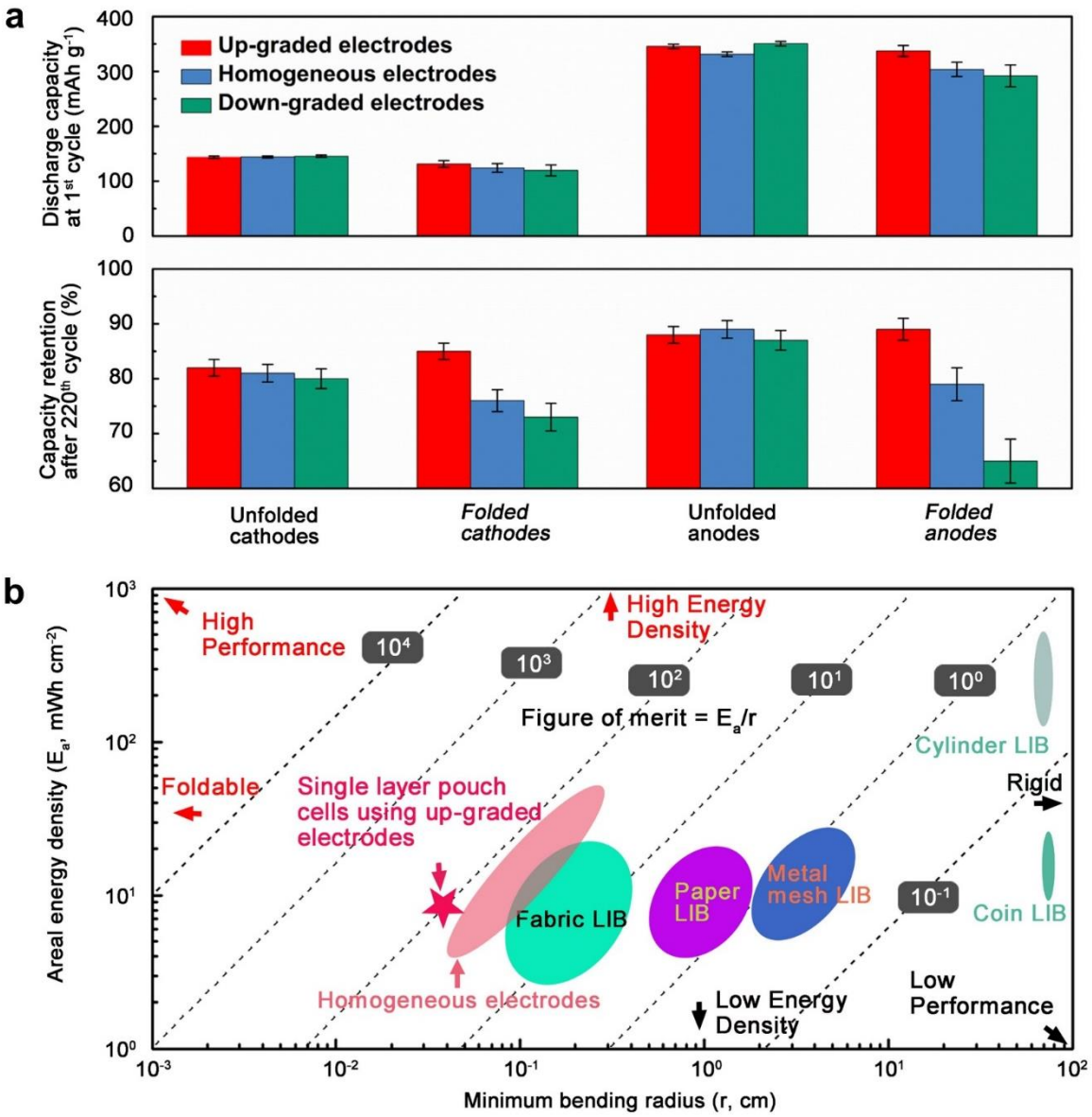

Figure 4. Comprehensive performance evaluation of up-graded, homogeneous and down-graded electrodes based on the mechanical and electrochemical behaviors. a and b) Electrochemical stability of the three folded electrodes. Before the cell assembly, the electrodes were folded convexly at three horizontal locations and three vertical locations. The bending radius was controlled by using standard stainless plates with known thickness. Detailed methods are given in the Supporting Information. a) For the discharge capacity in the first cycle, both the up-graded cathodes and anodes show slightly higher discharge capacity compared to homogeneous and down-graded electrodes. After 220 cycles, both the up-graded cathodes and anodes show obvious better retention compared to homogeneous and down-graded electrodes. b) A FOM based on the areal energy density versus bending radius (E_a/r) for standardizing the comparison of flexible LIBs. A higher FOM indicates better performance when comparing various battery systems with different thicknesses.

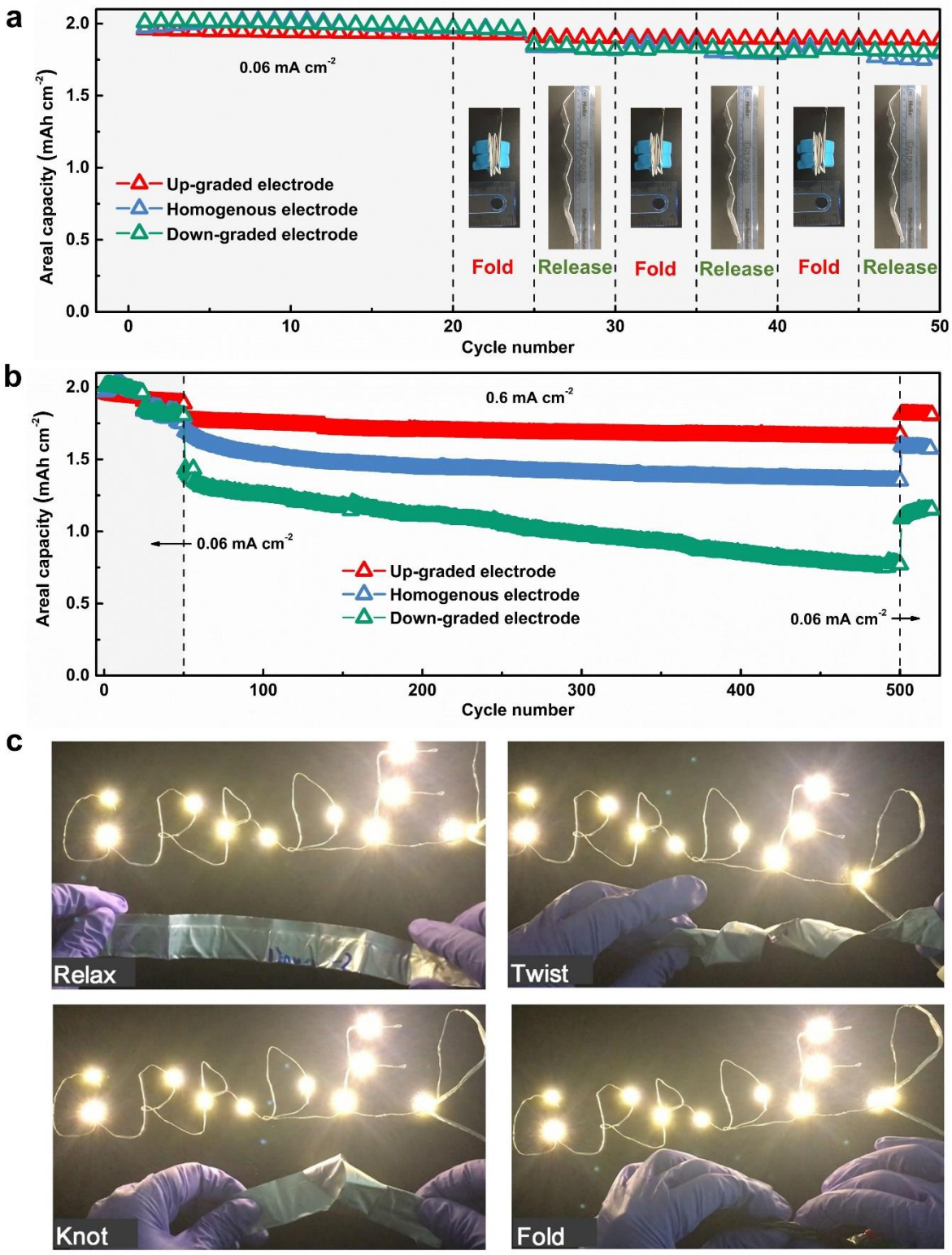

Figure 5. The stable power supply of the up-graded electrode-based pouch-type full cells under various conditions. a and b) The stability of pouch-type full cells (~ 60 mAh) under repeated folding and electrochemical cycling. a) the areal capacity in the first 50 cycles. The current density is set at 0.06 mA cm^{-2}. The bendability of the pouch cells was evaluated by subjecting them to three folding-releasing processes during cycling. b) The areal capacity retention in 520 cycles. The performance of the first 50 cycles is detailed in Figure (a). After

the 50th cycle, the pouch cells were cycled at the released state and current density of 0.6 mA cm^{-2} to evaluate the long-term influence on the previous folding-releasing process. After the 500th cycle, the current density is reduced to 0.06 mA cm^{-2}. c) Demonstration of pouch cells subjected to various deformation modes including twisting, folding and knotting. The pouch cells provide a stable power supply to the parallel LEDs during various conditions.

The table of contents entry

Mechano-graded electrodes with gradient-distributed maximum allowable strain are proposed to mitigate the mismatch between mechanical reliability and energy density for high-energy-density flexible lithium-ion batteries (LIBs). The up-graded electrode-based LIBs enable a remarkable figure of merit (FOM) value of 121.3 mWh cm^{-3}, proving the brilliant comprehensive performance of flexible high-energy-density LIBs.

Keywords: Mechano-graded electrodes, flexibility, energy density, lithium-ion batteries

Mechano-Graded Electrodes Mitigate the Mismatch between Mechanical Reliability and Energy Density for Foldable Lithium-Ion Batteries

*Xiang Ge, Shengkai Cao, Zhisheng Lv, Zhiqiang Zhu, Yuxin Tang, Huarong Xia, Hongwei Zhang, Jiaqi Wei, Wei Zhang, Yanyan Zhang, Yi Zeng, Xiaodong Chen**

TOC Figure